Inorganics **2014**, *2*, 313-333; doi:10.3390/inorganics2020313

OPEN ACCESS

inorganics

ISSN 2304-6740

www.mdpi.com/journal/inorganics

Article

Continuous Production of IF-WS_2 Nanoparticles by a Rotary Process

Fang Xu, Nannan Wang, Hong Chang, Yongde Xia and Yanqiu Zhu *

College of Engineering, Mathematics and Physical Sciences, University of Exeter, Exeter EX4 4QF, UK; E-Mails: f.xu@exeter.ac.uk (F.X.); nw291@exeter.ac.uk (N.W.); h.chang@exeter.ac.uk (H.C.); y.xia@exeter.ac.uk (Y.X.)

* Author to whom correspondence should be addressed; E-Mail: y.zhu@exeter.ac.uk; Tel.: +44-1392-723620; Fax: +44-1392-217965.

Received: 14 March 2014; in revised form: 6 May 2014 / Accepted: 4 June 2014 / Published: 13 June 2014

Abstract: This manuscript demonstrates the design, modification and initial investigation of a rotary furnace for the manufacturing of inorganic fullerene WS_2 nanoparticles. Different preparation methods starting with various precursors have been investigated, of which the gas-solid reaction starting with WO_3 nanoparticles was the most efficient technique. Furthermore, the influence of temperature, reaction time, and reaction gases *etc.* on the synthesis of inorganic fullerene WS_2 nanomaterials was investigated, and these parameters were optimised based on combined characterisations using XRD, SEM and TEM. In addition, the furnace was further modified to include a baffled tube, a continuous gas-blow feeding system, and a collection system, in order to improve the batch yield and realise continuous production. This technique has improved the production from less than 1 g/batch in a traditional tube furnace to a few tens of g/batch, and could be easily scaled up to industry level production.

Keywords: IF-WS_2 nanoparticles; large scale production; rotary process; WO_3 nanoparticles

---

1. Introduction

Inorganic nanotubes and inorganic fullerene-like (IF) structures of WS_2 were first discovered by Tenne *et al.* in 1992 [1], which has opened a challenging field for the synthesis and applications of numerous such layered structures, such as WS_2 [1], MoS_2 [2,3], BN [4], $NiCl_2$ [5], and *etc.* Various synthesis methods have been reported, such as the microwave treatment of $W(CO)_6$ (Tungsten carbonyl) reacting with H_2S (hydrogen sulphide) [6], ultrasonic irradiation of $W(CO)_6$ solution mixed with diphenylmethane and sulphur followed by heating at 800 °C [6], commercial WS_2 activation [7], iodine transport method [8], direct pyrolysis of WS_4^{2-} and CTAB (Cetyltrimethyl Ammonium Bromide) [9], and chemical vapour deposition [10]. Recently, IF-WS_2 nanoparticles and nanotubes have also been obtained from WCl_n and WO_xCl_y reacting with H_2S [11].

These IF-WS_2 and IF-MoS_2 nanomaterials, in addition to their significant mechanical, biocompatible and electronic properties, are excellent solid lubricants [12–20]. Accordingly, the incorporation of these nanomaterials into a proper matrix in composites will lead to new products with hugely improved physical and mechanical properties. Another extraordinary property of WS_2 nanostructures is their superb shock absorbing performance [21–23], which suggests an important field of application in lightweight and high performance protective composites [24]. Such applications will obviously demand large amounts of IF-WS_2 supply, however their synthesis was only obtained in gram level at the early stage, which was far too less for any practical work. More recently, Tenne's group has produced such IFs in large quantities by using new high tower reactors [25], hence realising a great industrial level success in nanomaterials. Nevertheless, an alternative, simple, versatile and yet effective process for the synthesis of such novel nanomaterials remains highly desirable.

Therefore, to develop an innovative, simple and scalable technique that is suitable for the continuous manufacture of IF-WS_2 nanomaterials becomes the primary aim of this work. From previous studies [25–27], where a deeper understanding of the formation mechanism of IF-WS_2 nanoparticles has been gained, it is found that the key technical barriers for scaling up of the IF-WS_2 lie in the powder agglomeration and superficial reaction, which occurs inevitably in a static gas–solid reaction. In order to achieve a large quantity manufacturing, effective measures should be taken to overcome these challenges.

This manuscript describes the design and modification of a rotary furnace, and the initial investigations in scaling up manufacturing of IF-WS_2 nanoparticles using the rotary furnace. Several processes starting with different precursors have been investigated, of which the gas–solid reaction using WO_3 nanoparticles as the precursor was the most efficient technique. The influence of temperature, reaction time, precursor types and reaction gases *etc.* on the synthesis of IF-WS_2 nanomaterials will be optimised. A significantly improved batch yield and a continuous process have been achieved.

2. Results and Discussion

2.1. Design and Modification of the Rotary Furnace

A novel rotary reactor has been designed for the manufacturing of IF-WS_2 nanomaterials. The rotary reactor was designed based on a conventional tube furnace. The furnace is 1 m long and has a working temperature up to 1200 °C, which ensures a long enough hot zone for complete reactions at the required temperatures.

Figure 1. Sketch of the rotary furnace. In a traditional static furnace, the WO_x particles stay still in the quartz tube at high temperature (800–900 °C), which leads to the dominance of 2H-WS_2 in the final products; whilst in the present furnace, the quartz working tubes are rotating, forcing the WO_3 and formed WS_2 nanoparticles to rotate and move during the process, resulting in better separated IF-WS_2 products at minimal agglomeration.

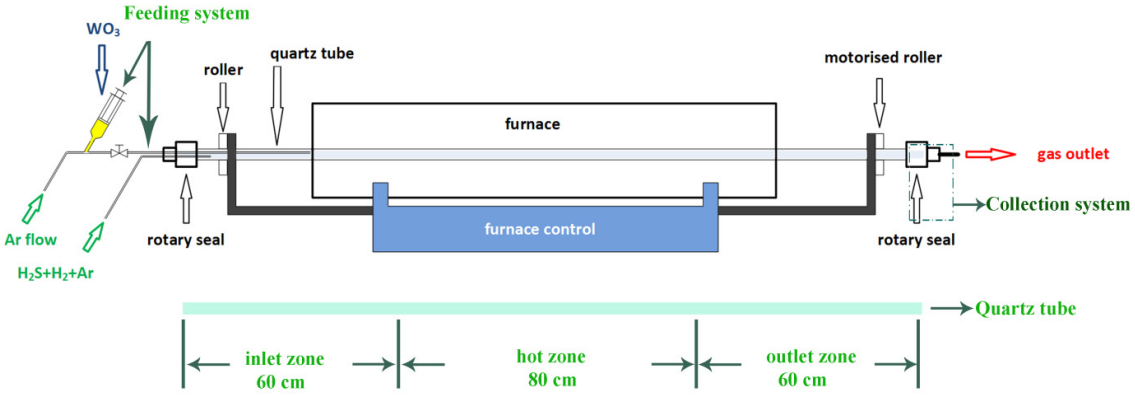

As shown in Figure 1, the rotary furnace consists of several essential parts: a basic tube furnace, a motorised driving and rolling system, an inclining system, a dynamic rotary seal system, a continuous feeding system and a collection system. The quartz working tube can be further modified to improve the batch yield. The working tube has inner diameter of 36 mm and outer diameter of 40 mm. Further modification was realised by adding two small oppositely positioned quartz rod blades of Ø5 mm to the inner wall (Figure S1), to provide extra forces driving the movement of powders inside the reactor. This would further eliminate particle agglomerations.

In order to extend the batch process to a continuous production, a continuous feeding system is required. In the current laboratory scale trial, after considering the existing screw feeding and piston feeding mechanisms [28–30], we adopted a simple pump piston feeder, which is more cost-effective. Actually, the current piston feeder under gravitation and gas blow works well in the current set up, since the slight vibration of the reactor helped avoid system blocking and keep a constant feeding. In industrial level, a proper, accurate screw feeder could be used to replace the current feeder. As shown in Figures 1 and S2, the feeder consists of a 20 mL push pump connected to a "T" junction, acting as the combined inlet blow gas and nanoparticle passage channel. The conceptual rotary furnace enables us to experiment with various parameters for optimal IF-WS_2 manufacture. A simple collection system has also been designed, as shown in the dashed box in Figure 1, which makes the process continuous.

The detailed schematic drawing of the collection system is shown in Figure S3. The key features of the practically assembled furnace are listed in Table 1.

Table 1. Key parameters of the designed furnace.

Temperature	Gas supply	Feeding level	Speed range	Inclination angle
0–1200 °C	Ar, H_2S, H_2	Up to 100 g*	0–350 rpm	−5 to 5°

*: depending on numbers of loaded pump container.

2.2. IF-WS_2 Synthesis by Different Methods

Different raw materials, including WO_3 and S mixture under H_2, ammonium paratungstate (APT) reacting with H_2S gas, and WO_3 reacting with H_2S, will be tested in this section.

2.2.1. WO_3 and S Reaction under H_2

The WO_3 precursor exhibits an average particle size of around 60 nm, having a monoclinic WO_3 structure (JCPDS No. 43-1035), as shown in Figures S4 and S5.

For the initial trial (experiment S1, as listed in Table 2), a composite powder of WO_3 and S at a molar ratio of a 1:10 was used as the precursor, and reacted under Ar/H_2 atmosphere at 800 °C, following the procedure described in Experimental Section 3.3.1. SEM images in Figure 2 show that very small nanoparticles and agglomerates were observed, with some nanoplatelets. However, the EDX spectrum shows that although WS_2 has formed, WO_x still dominates the products. This is also confirmed by XRD study as shown in Figure 3. In Figure 3, the peaks labelled with a triangle matched well with WS_2 (JCPDS No. 84-1398) [26], and all the other peaks labelled with a star could be assigned to $W_{18}O_{49}$ and $W_{20}O_{58}$. The highest WS_2 peak is at 2-theta 14.3°, corresponding to (002). The relatively low intensity of (002) plane for WS_2 reveals that only a few WS_2 layers have formed from the outside and leaving behind a WO_x core which has been reduced from WO_3 to $W_{18}O_{49}$ and $W_{20}O_{58}$. The presence of $W_{18}O_{49}$ and $W_{20}O_{58}$ is in agreement with previous studies [26,31–33], in which partially reduced $W_{20}O_{58}$ and thoroughly reduced $W_{18}O_{49}$ were formed during the oxide-to-sulphide conversion from WO_3 to IF- WS_2. There is no detectable S left in the products.

Figure 2. SEM images (**a**–**c**) and EDX spectrum (**d**) for products from experiment S1.

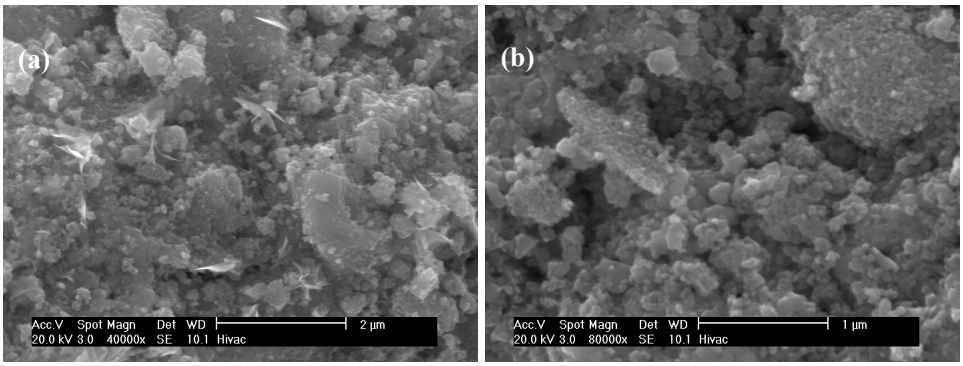

Figure 2. *Cont.*

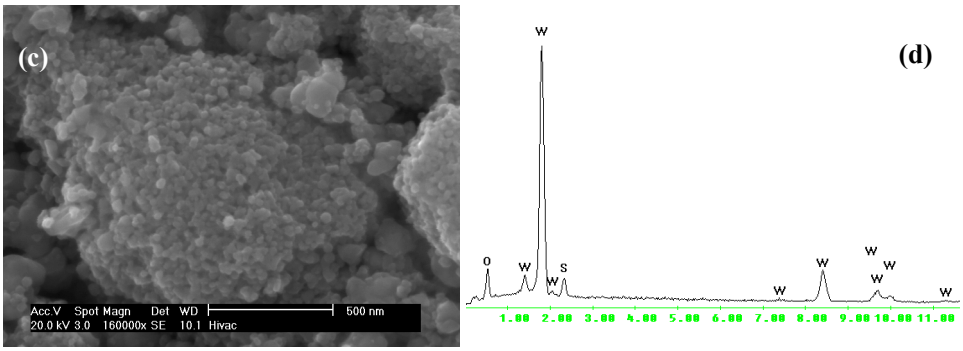

Figure 3. XRD pattern for WS_2 from experiment S1 (reaction of WO_3, S and H_2).

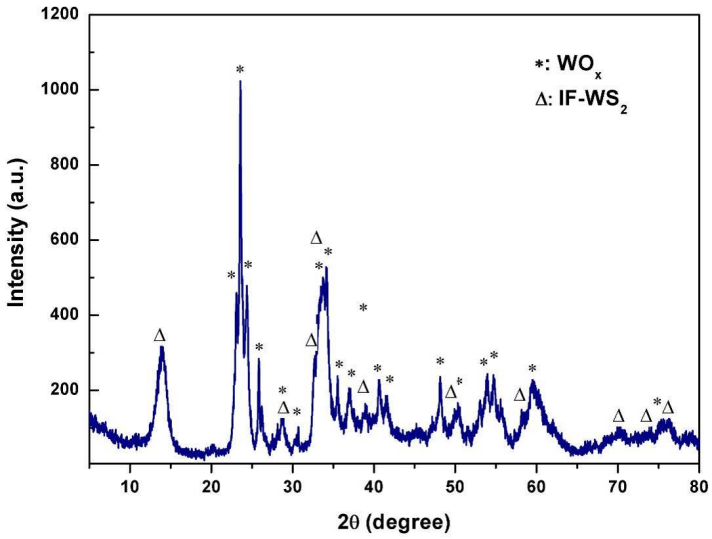

Although a molar ratio of 10:1 for S and W had been initially used, it seems that there was not enough S to react with the reduced WO_x core, because the S could not stay long enough in the hot zone. As soon as the powders reached the high temperature zone, the S would be sublimed and blown out of the high temperature zone, even under an optimised Ar/H_2 flow rate of 80 mL/min [34]. Therefore, the oxide-to-sulphide conversion could not be completed.

There are some similar works that used the same molar ratio of $S:WO_3$ = 10:1 [34], but only achieved a yield of less than 0.1 g per batch. It is obvious that this method is unsuitable for scaling up, as the product quality depends upon the quantity of WO_3 nanoparticles used and it is difficult to increase this for traditional static furnaces. To avoid the S loss, another batch process has also been reported recently [35], using solid $NaBH_4$ or $LiAlH_4$ as the H_2 releasing agent in a sealed ampoules. Again, these processes are not suitable for continuous production.

In this context, a continuous feeding and evaporation of S was tested, to compensate for the S loss during the reaction, as shown in Figure 1. The WO_3 and S mixed powder at a molar ratio of 1:10 was fed directly into the hot zone gradually using the pump, at elevated temperature, rather than pre-placed inside the quartz tube (experiment S2). The XRD analyses of the powders collected from both the inlet and hot zones have showed that only a few WS_2 layers formed and the majority remained as WO_x, and

S peaks were also present (peaks labelled with circle); although samples from the hot zone exhibited a more complete oxide-to-sulphide conversion (Figure S6).

Morphologically, the blue powders collected from the inlet zone consist of both very small particles and big aggregates, with some bright S residues, as shown in Figure 4a,b. At the relatively low temperature inlet zone, S could not completely react with the reduced WO_x, thus only a few layer WS_2 formed. For the hot zone samples (Figure 4c,d), some big agglomerates are visible, and they are indeed composed of nanoparticles after ultrasonic treatment.

Figure 4. SEM images of products collected from the inlet zone (**a** and **b**), and hot-zone (**c** and **d**) of experiment S2.

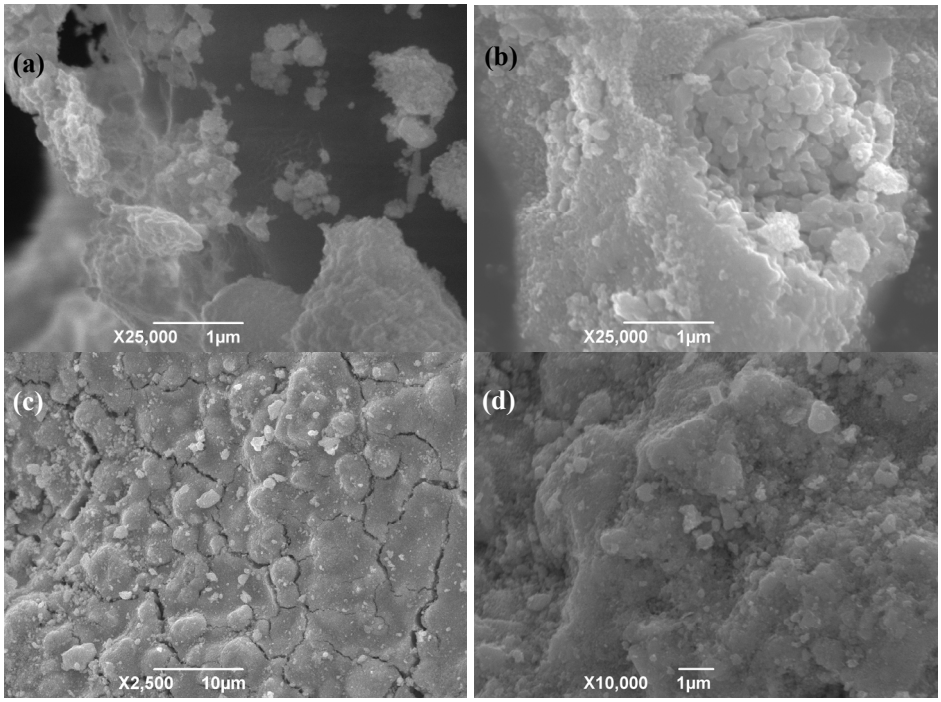

Therefore, although this technique has the potential for scaling up based on the continuous feeding system, the quality of the products is not high enough. Furthermore, when the temperature dropped below its boiling point, the S vapour could block the outlet gas pipes, which could be a practical issue. The large amounts of S consumption, although can be recycled, makes this process not cost effective.

2.2.2. APT as Precursor and H_2S as Reaction Gas

Since WO_3 nanoparticles were fabricated by the decomposition of APT, as described in the SI (Supplementary Information 2.2.2, Figures S7 and S8), and were a very valuable precursor for IF-WS_2 nanomaterials in previous two-step studies [1,25,26,36], *i.e.*, first decomposition of APT to form WO_3 then via sulphidisation to create IF-WS_2, it is thus interesting to combine the two steps together in our present set-up. This would be an advantage in terms of energy saving and process efficiency.

The as-received APT particles are crystals of several tens of μm in size, with nano-sized particles attached to the surface of these big crystals. Under high magnification, cracks and sub μm sized

particles could be observed at the corners of some damaged crystals, indicating that the APT crystals might be agglomerates of small pieces. Thus, prior to experiment (experiment AHS1), the APT particles were ultrasonic treated, to break the agglomerates into small pieces. The IF-WS_2 particles collected from hot zone are shown in Figure 5. On average, the agglomerates are smaller (Figure 5a), although some bigger aggregates which kept the original APT crystal shape were also observed, as shown Figure 5a,b. Higher magnification study shown in Figure 5c and d reveals the nanostructural feature within the agglomerates, and they are composed of both IF-WS_2 nanoparticles and nanoplatelets, roughly at the same proportion. XRD study (Figure 6) reveals that the hot zone products have very high intensity of WS_2 peaks, with only minor peaks of WO_x. In contrary, the outlet zone products contain a high portion of WO_x, owing to the shorter reaction time than those from the hot zone.

Figure 5. SEM images of samples from experiment AHS1, exhibiting the original shape and size of the APT (**a** and **b**), and the nanostructural feature within the agglomerates (**c** and **d**).

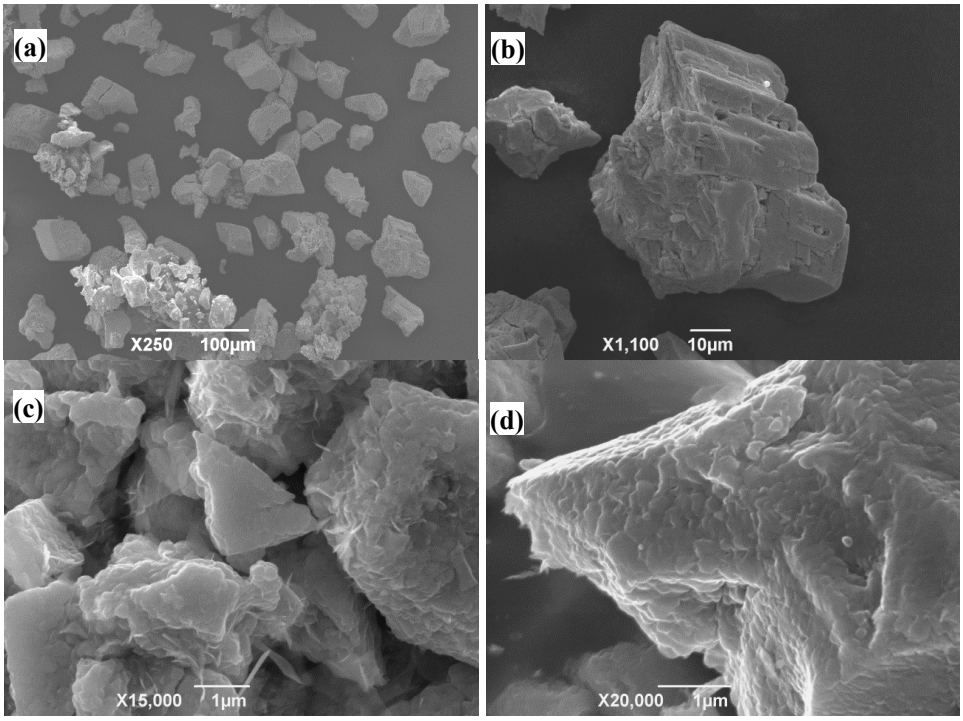

To form WO_x by decomposing APT, the temperature required will be above the melting point of tungsten oxide, e.g., 1200 °C to form WO_3 nanoparticles and 1350 °C for micro particles [37,38]. This allows for the tungsten oxide vapour to be brought to and deposited in the low temperature area. In the present process, the formed nanoparticles would then play the template role during subsequent sulphidisation, to form the IF-WS_2. Because of the different temperature requirements for the two steps, the direct IF-WS_2 synthesis using APT to react with H_2S seems to be an unsuitable choice for the present furnace.

Figure 6. XRD patterns of samples collected from different areas (**a**, outlet and **b**, hot zone) in experiment AHS1.

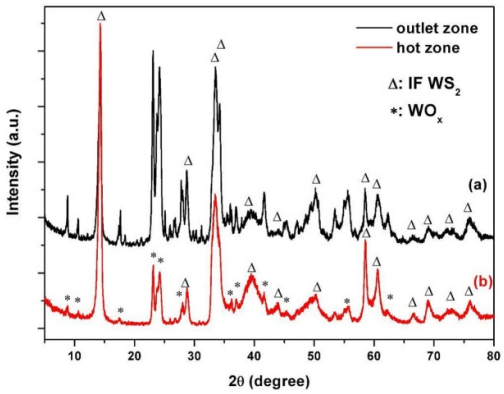

2.2.3. WO_3 and H_2S Synthesis of WS_2 Nanomaterials

Figure 7 shows the SEM results of experiment W1. A feature of nanoparticle domination is visible, with big agglomerates (Figure 7a). The semi-spherical IF-WS_2 nanoparticles exhibit different sizes (Figure 7b): the tiny ones have diameters of <50 nm which are the same as the WO_3 precursor; whilst the big ones are about 100–200 nm, possibly merging from two or more nanoparticles. The presence of nanosheets or nanoplatelets amongst nanoparticles can be seen from Figure 7c (arrowed). XRD investigation confirms that the majority of the products are IF-WS_2 nanoparticles, with left-shifted (002) peak and broadened (103) and (105) peaks [3], Figure 7d. Tiny peaks at 23–25 degrees (labelled with a star) can be assigned to WO_x core residue. XRD comparison between the produced IF-WS_2 and the commercial 2H-WS_2 has been presented in the Supplementary Information, as Figure S9, where the differences between XRD pattern of the resulting IF-WS_2 and 2H-WS_2 are discussed in detail.

Figure 7. SEM images (**a**–**c**) and XRD pattern (**d**) of IF-WS_2 synthesised using the rotary process.

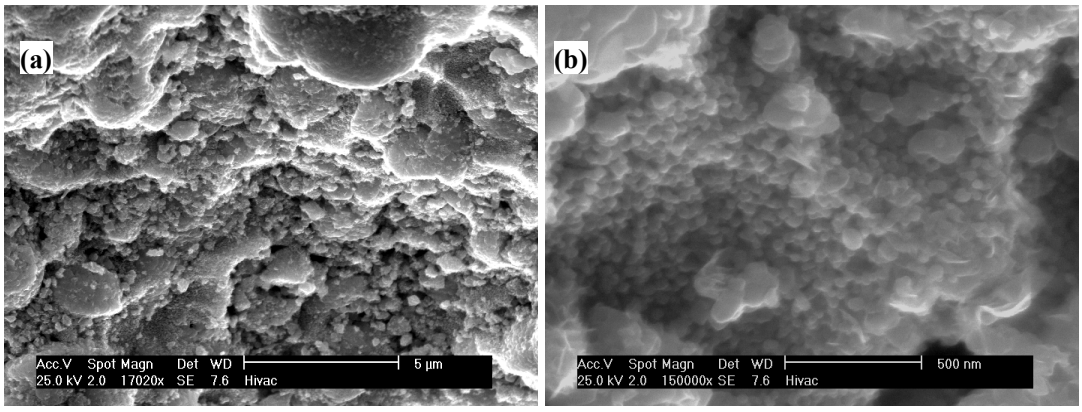

Figure 7. *Cont.*

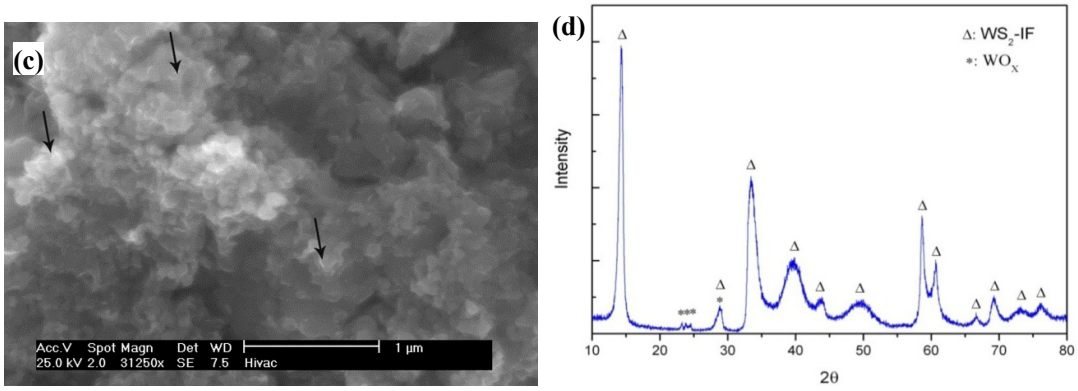

Further TEM examination shows that the sample contains both nanoparticles and nanosheets/nanoplatelets (Figure 8a). Indeed, the IFs exhibit the multi-layered, hollow core characteristics, being the dominant phase. Some particles followed the original shape of their oxide precursor, appearing in a spherical, seamless, and close-caged structure (arrows A); whilst some displayed a peanut-like structure (arrows B) or a long elliptical shape (arrow C). These unusual particles were possibly co-formed from adjacent WO_3 nanoparticles that fused together during the heating. The continuous contour of WS_2 layers suggests that these particles must have fused together first, then the oxide-to-sulphide conversion occurred. This observation can also explain the different particle sizes observed under SEM, as shown in Figure 8b,c. The products, regardless of their different shapes, possess a hollow core and a generally equal d(002) spacing of 0.62 nm for IF-WS_2.

Figure 8. TEM images of the WS_2 synthesised using the rotary process (**a**–**d**; b is a zoomed-in image of framed area in a).

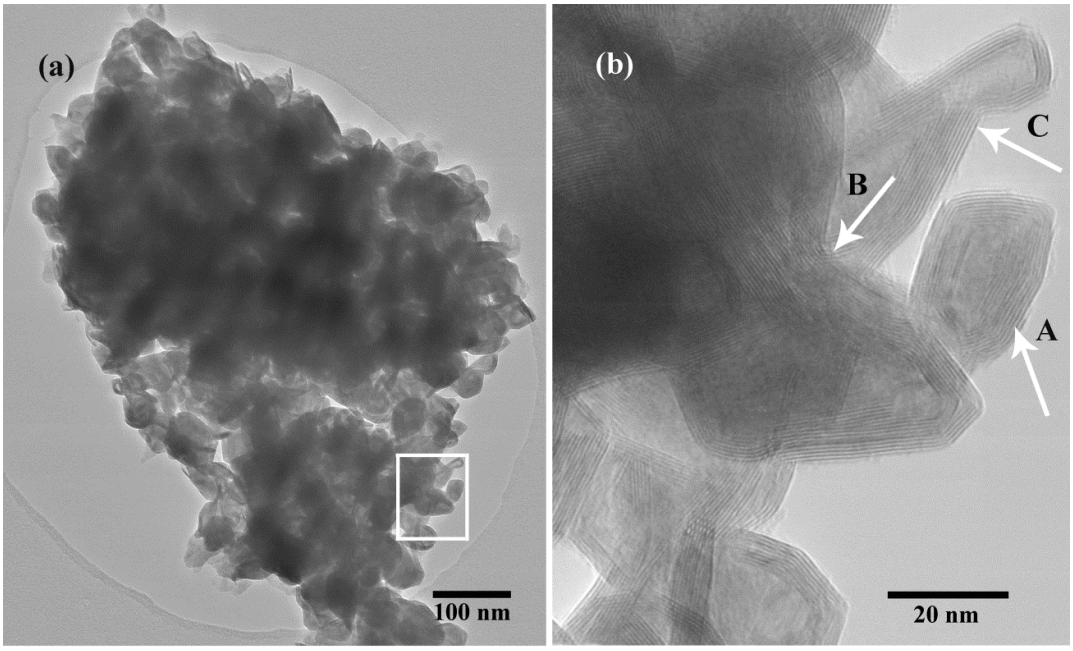

Figure 8. *Cont.*

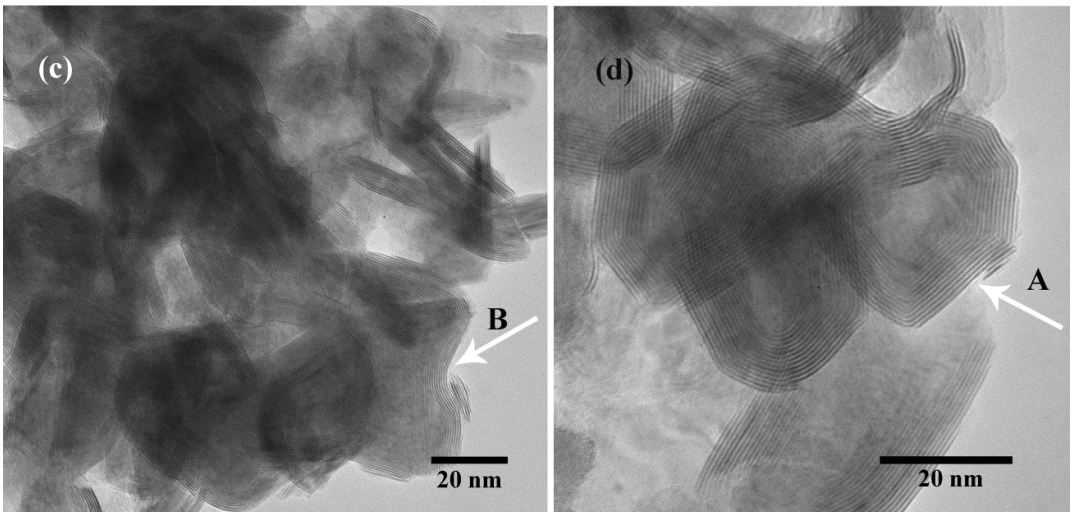

These characterisations of the products have confirmed that IF-WS_2 is the dominant phase in the product with high quality. This shows the great potential for the production of IF-WS_2 at large quantities and high quality, using the present rotary process. Further investigations will focus on quality assessment and quantity improvement.

2.3. Optimization of IF-WS_2 Synthesis from WO_3 Precursor and H_2S Gas

2.3.1. Reaction Time

After applying fixed rotary speed and temperatures, the influence of different reaction times were assessed, as listed in Table 3. Figure 9 shows the resulting products exhibiting similar features as described earlier. For the 10 min product (experiment A, Figure 9a), the oxide was just about to be reduced. Only the outer layer finished the oxide-to-sulphide conversion, whilst the inner core remained intact, which is in line with Tenne *et al.*'s TEM observation [26]. For the 50 min sample (Experiment B, Figure 9b), by analysing the intensity changes of the diffraction peaks, it is clear that the oxide particles have mostly converted to IF-WS_2 and there is much less suboxide left in the core. Similarly, after an 80 min reaction, the WO_x peaks at around 23–25 degrees continued to be reduced, and more and more IF-WS_2 layers formed, suggesting an almost complete conversion. Further increase of the reaction time leads to no significant differences in the XRD profiles, and there is almost no peak detected for any tungsten oxide. Thus, a 110 min reaction time is believed to be sufficient for a thorough sulphidisation.

Figure 9. XRD profiles of samples from experiments A–F, demonstrating the effect of different reaction time at 800 °C from 10–170 min.

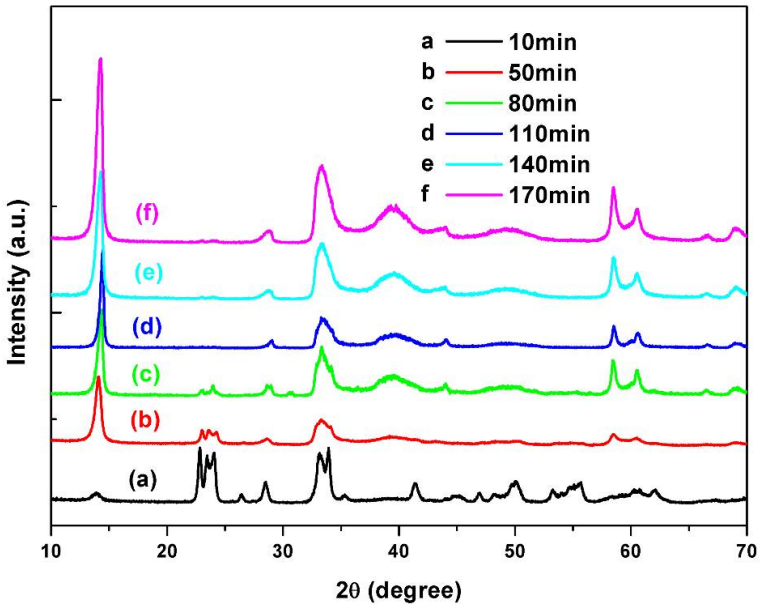

2.3.2. Reaction Temperatures

Of the experiments listed in Table 3, batches C and G used similar parameters, except for the temperature which was 900 °C for batch G but 800 °C for batch C. From 900 °C, the intensity of the resulting IF-WS_2 (Figure 10) is much higher than that from 800 °C (Figure 10), confirming more WS_2 layers formed at higher temperatures, under the same reaction time of 80 min.

Figure 10. XRD profiles of samples from batch C (800 °C, **red curve**) and G (900 °C, **black curve**) and their SEM images.

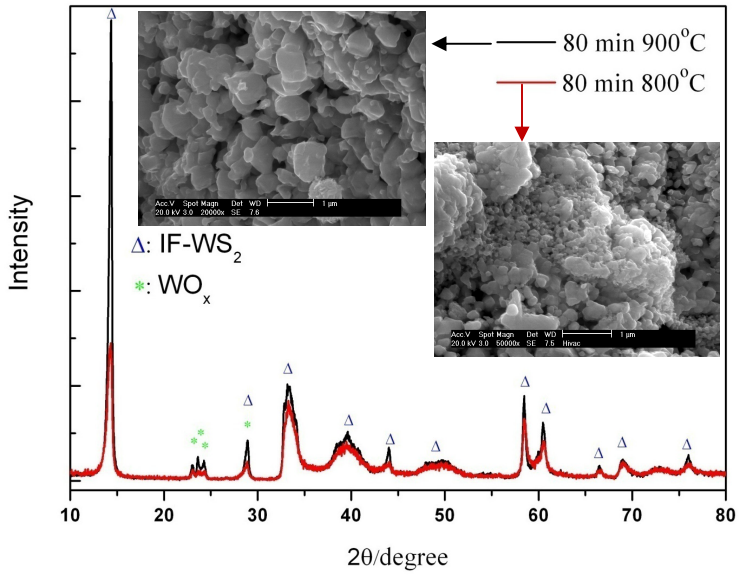

2H-WS_2 flakes were presented in both samples (Figure 11), however there was much more 2H-WS_2 formed in batch G, possibly due to the higher temperature which made agglomeration more severe. The IF-WS_2 particles are also considerably larger in batch G, some of which exhibited a diameter of 300–500 nm, in contrast to 100–200 nm in experiment C. This observation accounted for the extremely high relative intensity of the (002) peak for sample G.

Figure 11. SEM pictures of samples from batch C (**a**–**c**) and batch G (**d**–**f**).

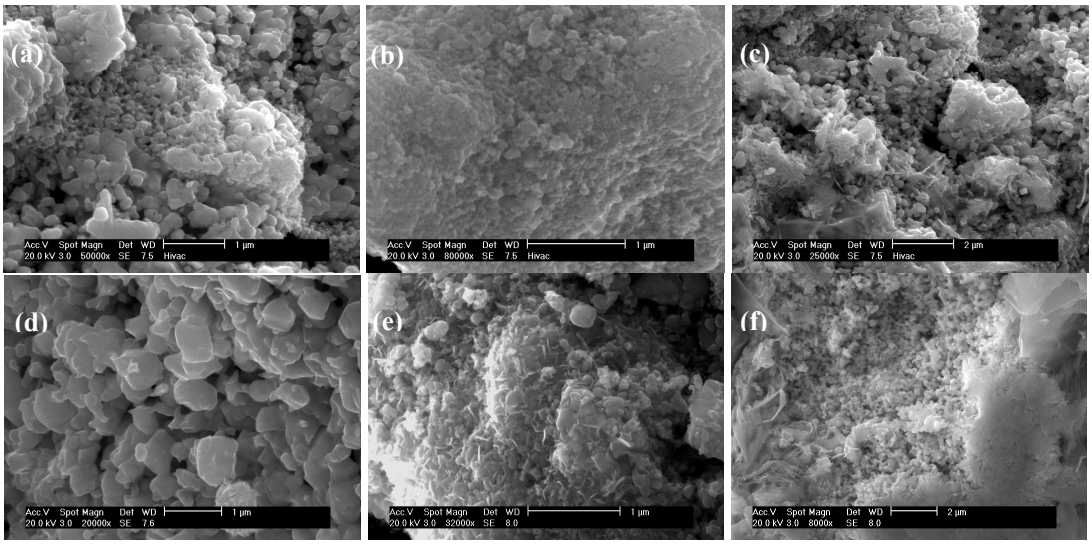

Actually, when compared with other experiments from A–G, the quality of products from batch G (the highest temperature used, 900 °C) are the worst of all, regardless of different reaction times. Thus, temperature is considered to be one of the most significant parameters directly linked with agglomeration in the present process.

2.3.3. Influence of H_2

H_2 was introduced to some experiments (e.g., experiment H1), to promote the WO_x and H_2S reaction. In these samples, the majority of the product is IF-WS_2 of less than 100 nm in size (Figure 12a,b), with very few 2H-WS_2 (Figure 12c). Rod shaped WS_2 were also observed occasionally, as shown in Figure 12d. Indeed, the formation of IF-WS_2 nanotubes was previously reported in the presence of H_2 in the reaction gases [27,39,40]. The XRD profile looks identical to those without H_2. Overall, the results show a positive effect when H_2 was added to the reaction gas.

Similarly, many previous studies have indicated that, during the conversion from WO_3 to WS_2, the WO_3 was first reduced to tungsten suboxide such as $W_{20}O_{58}$, $W_{18}O_{49}$ *etc.* From a localized view, the S replaced the O as soon as the reduction of tungsten oxide initiated. From an overall point of view, the reduction and sulfurization processes must have taken place in parallel [26,31–33]. Thus, the addition of H_2 into the reaction gases would accelerate the reduction of tungsten oxides and speed up the subsequent sulphidization, thereby leading to prompt formation of the WS_2 layers on the oxide surface. Since the early formation of an inert WS_2 layer would prohibit the diffusion and agglomeration of

neighbouring nanoparticles, H_2 introduction helped prevent particles from agglomeration, hence effectively reducing the chance for the formation of 2H-WS_2.

Figure 12. SEM images of samples involving H_2 in reaction, showing particles less than 100 nm (**a**–**c**), and the presence of nanotubes (**d**).

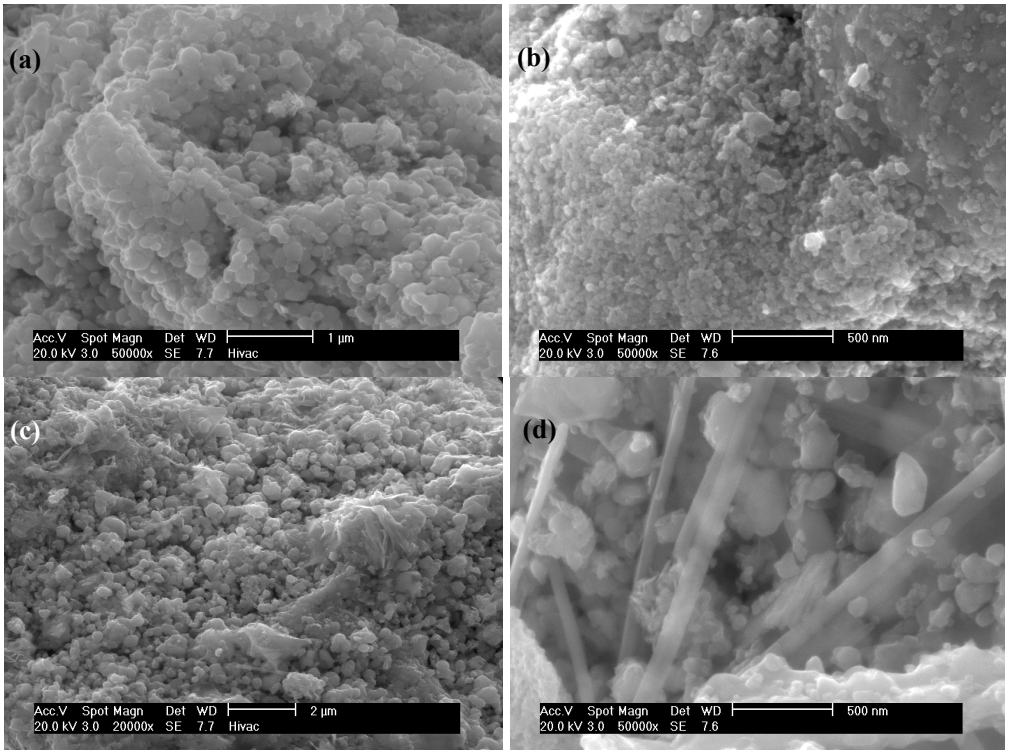

2.4. Further Refinement and Modification

2.4.1. IF-WS_2 Synthesis Using a New Baffled Quartz Tube

To improve the batch yield, a new baffled quartz tube was designed and adopted for the experiment (Figure S1). Based on previous optimal parameters, changes were made to reflect the significantly increased precursor from 6–18 g. For example, the gas rate of H_2 and H_2S, the reaction time and inclination angle *etc.* were finely adjusted in experiments B1–B3.

For the new baffled tube, a bigger inclination angle was required at the beginning of the experiment in order to drive the particles towards the hot zone, otherwise they would only move around rather than move forward. As soon as all the particles marched into the hot zone, the angle could be decreased to zero for better reaction. In a typical experiment, 18 g WO_3 nanoparticles were used with an initial inclination angle of 5 degrees, and H_2: H_2S: Ar ratio of 10:30:160 for the whole process. After the experiment, 15 g out of the 18 g were collected from the hot zone. By reducing the H_2 gas content in the flow in the later stage of the reaction (experiment B3), the amount of WS_2 nanotubes has been dramatically decreased, and they were much shorter (compared to experiments B1 and B2), Figure 13a. The dominant IF-WS_2 nanoparticles appeared to be uniform, fine and spherical, with diameters <100 nm

(Figure 13b). Their XRD pattern is very promising, with strong WS_2 peaks and very tiny WO_x signals, which is again indicative of a good sulphidisation.

Figure 13. SEM images for samples collected from the hot zone of experiment B3, revealing the existence of a small amount of nanotubes (**a**), and the fine and uniform IF-WS_2 (**b**).

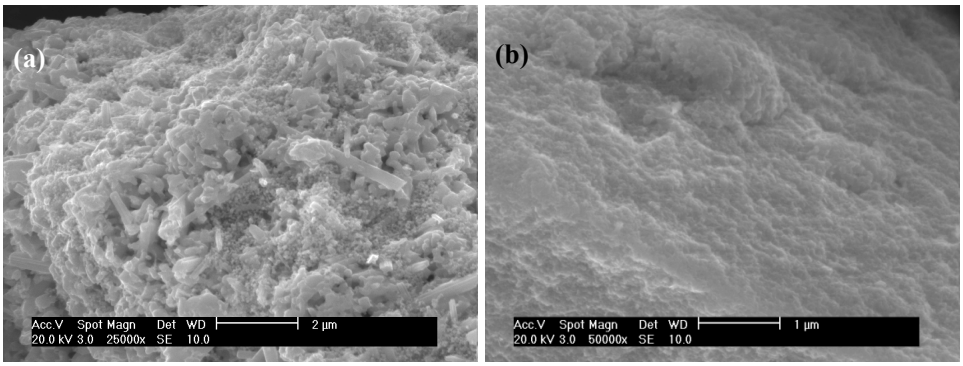

Figure 14. TEM images for samples collected from the hot zone of experiment B3, demonstrating the overall distribution of particle (**a**) and the multi-layered characteristics of different particles (**b**–**d**).

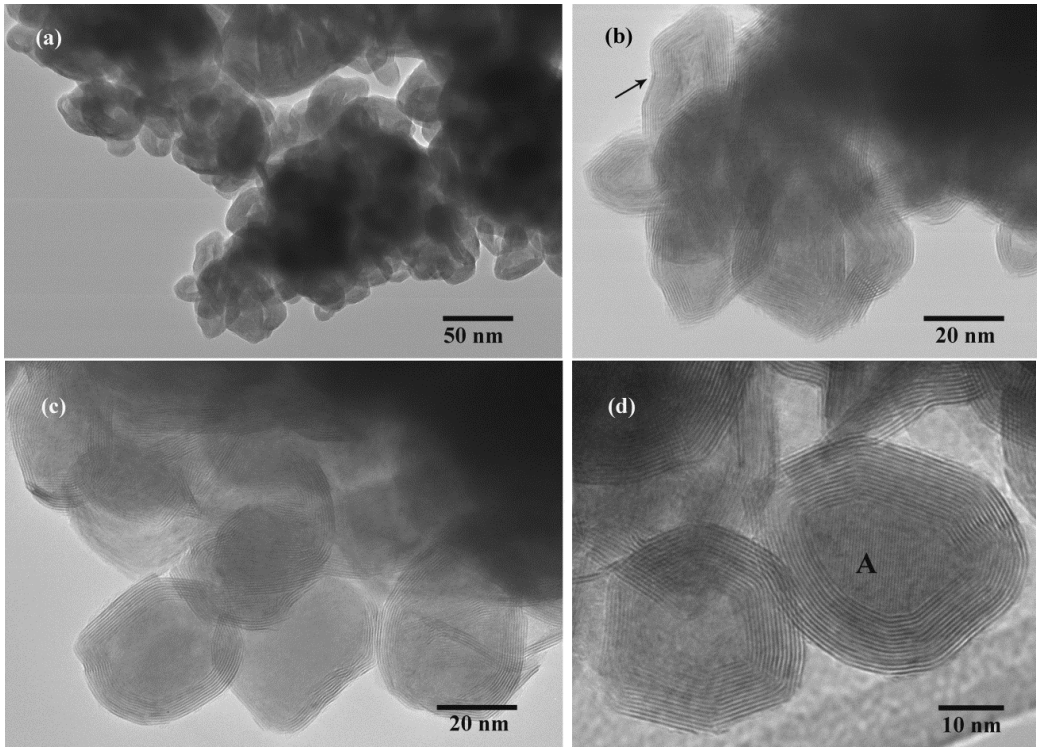

TEM characterisation for sample B3 (Figure 14) further confirm the dominant nature of the IF-WS_2, with sizes ranging from below 50 nm to up to 100 nm. Figure 14b also demonstrates that some particles coalesced from two or three nanoparticles, exhibiting a peanut shape (arrowed). Those single particles are always <50 nm. Figure 14b–d show high resolution images of well-crystallised IF-WS_2

particles, which again reveal their typical hollow core and seamless shell layer features. Some particles still possess a residue WO_x core (particle A in Figure 14d). Nevertheless, the new baffled working quartz tube was most promising, enabled a yield improvement from 5 g–15 g per batch whilst successfully maintaining the products quality. However, as the mixing efficiency drops with the filling degree [41], a too high amount of WO_3 precursor input would lead to less effective mixing and thus compromise the quality of the final product. Thus, the batch yield and product quality are limited by the quantity of the precursors loaded at the beginning of each batch. Further improvement is still necessary.

2.4.2. A Continuous Feeding System

In this feeding system (Figure 1), the WO_3 precursor was first stored in a pump and then introduced to the system by gravity and gas-blow. A single long feeding tube was used to act as the extended pathway for WO_x particles directly blown into the system (as shown in Figures 1 and S2), while the reaction gases were fed in by a separated tube. The new design was tested (FB1), and the result showed a complete conversion of WO_x into IF-WS_2 for particles from the hot zone (Figure S10). The products were quite uniform, with sizes no more than 100 nm (Figure S11).

The process was further modified to simulate a real, continuous one, by immediately replacing the empty pump with a full one (FB2). All other experimental parameters made no alteration to FB1, except for the longer feeding time. In this case, around 50 g samples were collected from the hot zone. TEM images of the hot zone sample from FB2 were shown in Figure 15. Majority nanoparticles of around 50 nm in size are displayed in Figure 15a,c, some from 20 nm to almost 100 nm are exhibited in Figure 15b. A typical IF-WS_2 particle with a hollow core and around 15 seamless layers is shown in Figure 15d.

Figure 15. TEM images for particles collected from the hot zone from experiment FB2, showing overall uniformity of particles (**a** and **c**) and detailed closed-cage feature under high resolution (**b** and **d**).

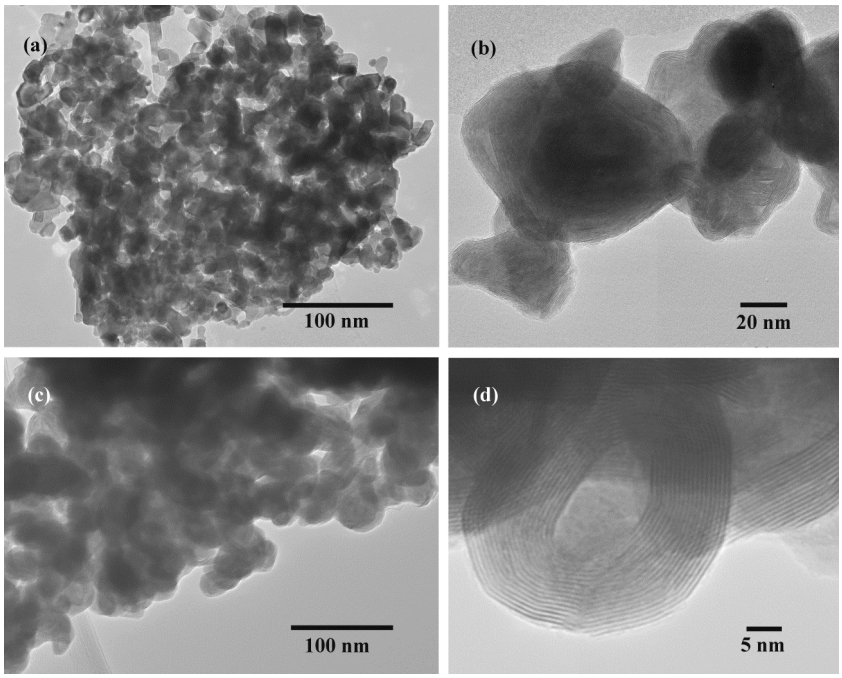

To summarise, the continuous feeding system has been proven a success and has improved the yield of IF-WS_2 to several tens of grams per batch, without having an obvious compromise on quality. Technically, the feeding of precursor could be simply continued by reloading; however, a longer reaction time would be required. In an industry environment, where a proper sample collection system is easily available, an automated reaction would not be a limitation. This reactor is easily adaptable as a whole continuous rotary process for the scaling up production of IF-WS_2 nanoparticles, using a proper metallic working tube.

3. Experimental Section

3.1. Materials

Commercial tungsten trioxide powder used as precursor for IF-WS_2 nanomaterials was monoclinic WO_3 powder (light yellow, with size < 100 nm, purity 99%, Sigma-Aldrich, UK). Ammonium paratungstate (APT, $(NH_4)_{10}H_2(W_2O_7)_6{\cdot}xH_2O$, 99.99%) particles used to produce WO_x nanoparticles were bought from Sigma-Aldrich, UK. Sulphur (S, sublimed, 100 mesh, 99.5%) was purchased from Cole-Parmer, UK. For comparison with the produced IF-WS_2 nanoparticles, 2H-WS_2 platelets (powder, 2 μm, 99%) were also bought from Sigma-Aldrich, UK.

3.2. Experimental Set-Up

Based on the furnace shown in Figure 1, the parameters for the experiments were optimized through a series of experiments, such as different reaction temperatures, reaction time, reaction gas atmosphere, modification of working tube, and a new feeding system. The optimization experiments were carried out without the feeding system, unless specifically stated. The products were collected from different areas separately, where the central 80 cm part of the quartz tube in the heated zone was defined as hot zone, the 60 cm part close to the gas inlet end was named as the inlet zone, and similarly the outlet zone, as also shown in Figure 1. Note that the reaction time could be varied mostly through the inclination of the quartz reactor, and the motor could drive the working quartz tube both clockwise and anti-clockwise. In such a way, the particles could be moved either backwards or forwards as required, to achieve sufficiently long reaction time.

The morphology and chemical composition of the as-produced IF-WS_2 nanoparticles were analysed by XRD, SEM and TEM. The TEM samples were prepared via an ultrasonic treatment of the nanoparticles (randomly collected from hot zone) for 5 min in acetone, and the resultant uniform suspension was pipetted onto a holey carbon coated copper grid (300 mesh, Agar).

3.3. IF-WS_2 Synthesis by Different Methods

3.3.1. Synthesis of IF-WS_2 Nanoparticles from Mixed WO_3 and S Powder with H_2

Two typical types of experiment were carried out to synthesize the IF-WS_2, starting from mixed WO_3 and S powder with H_2 (experiments S1 and S2). In experiment S1, around 6 g WO_3 and S composite powder at a molar ratio of 1:10 was placed into the inlet area. Ar gas was used to purge the quartz tube at 50 mL/min for 30 min, after the system was properly assembled and sealed. The

working tube started rotating from 600 °C, at which point H_2 (80 mL/min) and Ar (30 mL/min) gases were also introduced. The reaction at 800 °C lasted for 1 h. Similarly, experiment S2 was carried out by adopting a continuous S feeding system.

3.3.2. Synthesis of IF-WS_2 Nanoparticles from APT Precursor with H_2S Gas

Six g APT were ultrasonically treated and dried before being placed into the centre of the quartz tube for the experiment (AHS1). Ar (50 mL/min) was flushed for 30 min before the furnace was switched on. H_2S flowing was started from 550 °C till the end of the process, at a rate of 12 mL/min. The whole reaction lasted for 2 h at 800 °C, at a fixed Ar flow rate of 100 mL/min.

Except for experiments on various reaction times (summarised separately), all other experimental parameters are summarised in Table 2.

Table 2. Example parameters used for the synthesis of IF-WS_2.

	Precursor put in (g)	**Gas feed Rate (H_2:H_2S:Ar) (mL/min)**	**Reaction time (min)**	**Reaction temperature (°C)**
S1	6	80:0:30	60	800
S2	12	80:0:30	120	800
AHS1	6	0:12:100	120	800
W1	6	0:12:100	90	800
H1	6	8:12:100	90	800
B1	18	10:30:160	120	800
B2	18	20:30:100	120	800
B3	18	20:30:100 10:30:100	120	800
FB1	50	50:50:100 0: 25:100	180	800
FB2	100	50:50:100 0:25:100	300	800

3.3.3. Synthesis of IF-WS_2 Nanoparticles WO_3 and H_2S Gas

The synthesis of WS_2 nanomaterials from reaction of WO_3 and H_2S gas was similar to that from WO_3 and S (Section 3.3.1), except for the H_2 gas being replaced by H_2S. The first trial was named experiment W1 (Table 2).

Table 3. Example parameters used for the synthesis of IF-WS_2 with varying reaction times.

	WO_3 Precursor (g)	**Gas feed rate (H_2S:Ar) (mL/min)**	**Reaction time (min)**	**Reaction temperature (°C)**
A	6	12:100	10	800
B	6	12:100	50	800
C	6	12:100	80	800
D	6	12:100	110	800
E	6	12:100	140	800
F	6	12:100	170	800
G	6	12:100	80	900

Table 3 summarises the parameters used for a series of experiment at a fixed rotation speed of 140 rpm, with reaction time varying from 10–170 min.

4. Conclusions

Based on the built rotary system, the large scale manufacture of IF-WS_2 nanoparticles has been realised. Several synthesis methods have been studied, and the process starting with WO_3 precursor and H_2S reaction gas is most successful. Systematic studies have been carried out to optimise the parameters for IF-WS_2 nanoparticle production, including precursor types, reaction temperatures, reaction time and reaction gases. Further refinements by modifying the working quartz tube and the feeding system have made the continuous manufacturing possible. This new technique, as a simple alternative to the fluidised bed method, has improved the yield of IF production from less than 1 g/batch using a traditional tube furnace to a few tens of g/batch. This process is easily scalable to industry production level, by incorporating existing equipment.

Acknowledgments

The authors thank EPSRC (Engineering and Physical Sciences Research Council, UK) for financial support.

Author Contributions

Fang Xu designed, tested and modified the rotary furnace, conducted the experiments and drafted the manuscript; Nannan Wang and Hong Chang helped with some experiments and particle characterisations; Yongde Xia contributed to the data analyses; Yanqiu Zhu oversaw the entire project progress, and was the project leader.

Conflicts of Interest

The authors declare no conflict of interest.

References

1. Tenne, R.; Margulis, L.; Genut, M.; Hodes, G. Polyhedral and cylindrical structures of tungsten disulphide. *Nature* **1992**, *360*, 444–446.
2. Margulis, L.; Salitra, G.; Tenne, R.; Talianker, M. Nested fullerene-like structures. *Nature* **1993**, *365*, 113–114.
3. Feldman, Y.; Wasserman, E.; Srolovitz, D.J.; Tenne, R. High rate, gas phase growth of MoS_2 nested inorganic fullerenes and nanotubes. *Science* **1995**, *267*, 222–225.
4. Chopra, N.G.; Luyken, R.J.; Cherrey, K.; Crespi, V.H.; Cohen, M.L.; Louie, S.G.; Zettl, A. Boron nitride nanotubes. *Science* **1995**, *269*, 966–967.
5. Rosenfeld, H.Y.; Grunbaum, E.; Tenne, R.; Sloan, J.; Hutchison, J.L. Cage structures and nanotubes of $NiCl_2$. *Nature* **1998**, *395*, 336.

6. Vollath, D.; Szabo, D.V. Synthesis of nanocrystalline MoS_2 and WS_2 in a microwave plasma. *Mater. Lett.* **1998**, *35*, 236–244.
7. Mackie, E.B.; Galvan, D.H.; Adem, E.; Talapatra, S.; Yang, G.L.; Migone, A.D. Production of WS_2 nanotubes by an activation method. *Adv. Mater.* **2000**, *12*, 495–498.
8. Remskar, M.; Skraba, Z.; Regula, M.; Ballif, C.; Sanjine's, R.; Levy, F. New crystal structures of WS_2: microtubes, ribbons, and ropes. *Adv. Mater.* **1998**, *10*, 246–249.
9. Li, Y.D.; Li, X.L.; He, R.R.; Zhu, J.; Deng, Z.X. Artificial lamellar mesostructures to WS_2 nanotubes. *J. Am. Chem. Soc.* **2002**, *124*, 1411–1416.
10. Li, X.L.; Ge, J.P.; Li, Y.D. Atmospheric pressure chemical vapor deposition: An alternative route to large-scale MoS_2 and WS_2 inorganic fullerene-like nanostructures and nanoflowers. *Chem. A Eur. J.* **2004**, *10*, 6163–6171.
11. Margolin, A.; Deepak, F.L.; Popovitz-Biro, R.; Bar-Sada, M.; Feldman, Y.; Tenne, R. Fullerene-like WS_2 nanoparticles and nanotubes by the vapor-phase synthesis of WCl_n and H_2S. *Nanotechnology* **2008**, *19*, doi:10.1088/0957-4484/19/9/095601.
12. Seifert, G.; Terrones, H.; Terrones, M.; Jungnickel, G.; Frauenheim, T. Structure and electronic properties of MoS_2 nanotubes. *Phys. Rev. Lett.* **2000**, *85*, 146–149.
13. Dominko, R.; Arcon, D.; Mrzel, A.; Zorko, A.; Cevc, P.; Venturini, P.; Gaberscek, M.; Remskar, M.; Mihailovic, D. Dichalcogenide nanotube electrodes for Li-Ion batteries. *Adv. Mater.* **2002**, *14*, 1531–1534.
14. Kaplan-Ashiri, I.; Tenne, R. Mechanical properties of WS_2 nanotubes. *J. Cluster Sci.* **2007**, *18*, 549–563.
15. Rapoport, L.; Feldman, Y.; Homyonfer, M.; Cohen, H.; Sloan, J.; Hutchison, J.L.; Tenne, R. Inorganic fullerene-like material as additives to lubricants: Structure–function relationship. *Wear* **1999**, *225–229*, 975–982.
16. Kaplan-Ashiri, I.; Cohen, S.R.; Gartsman, K.; Ivanovskaya, V.; Heine, T.; Seifert, G.; Wiesel, I.; Wagner, H.D.; Tenne, R. On the mechanical behavior of WS_2 nanotubes under axial tension and compression. *Proc. Natl. Acad. Sci.* **2006**, *103*, 523–528.
17. Rapoport, L.; Bilik, Y.; Feldman, Y.; Homyonfer, M.; Cohen, S.R.; Tenne, R. Hollow nanoparticles of WS_2 as potential solid-state lubricants. *Nature* **1997**, *387*, 791–793.
18. Hou, X.H.; Shan, C.X.; Choy, K.L. Microstructures and tribological properties of PEEK-based nanocomposite coatings incorporating inorganic fullerene-like nanoparticles. *Surf. Coat. Technol.* **2008**, *202*, 2287–2291.
19. Brown, S.; Musfeldt, J.L.; Mihut, I.; Betts, J.B.; Migliori, A.; Zak, A.; Tenne, R. Bulk *vs.* nanoscale WS_2: Finite size effects and solid-state lubrication. *Nano Lett.* **2007**, *7*, 2365–2369.
20. Frey, G.L.; Elani, S.; Homyonfer, M.; Feldman, Y.; Tenne, R. Optical-absorption spectra of inorganic fullerene like MS_2 (M = Mo, W). *Phys. Rev. B* **1998**, *57*, 6666–6671.
21. Zhu, Y.Q.; Sekine, T.; Li, Y.H.; Wang, W.X.; Fay, M.W.; Edwards, H.; Brown, P.D.; Fleischer, N.; Tenne, R. WS_2 and MoS_2 inorganic fullerenes—super shock absorbers at very high pressures. *Adv. Mater.* **2005**, *17*, 1500–1503.

22. Zhu, Y.Q.; Sekine, T.; Li, Y.H.; Fay, M.W.; Zhao, Y.M.; Poa, C.H.P.; Wang, W.X.; Roe, M.J.; Brown, P.D.; Fleischer, N.; *et al.* Shock-absorbing and failure mechanisms of WS_2 and MoS_2 nanoparticles with fullerene-like structures under shock wave pressure. *J. Am. Chem. Soc.* **2005**, *127*, 16263–16272.
23. Zhu, Y.Q.; Sekine, T.; Brigatti, K.S.; Firth, S.; Tenne, R.; Rosentsveig, R.; Kroto, H.W.; Walton, D.R.M. Shock-wave resistance of WS_2 nanotubes. *J. Am. Chem. Soc.* **2003**, *125*, 1329–1333.
24. Hogg, P.J. Composites in Armor. *Science* **2006**, *314,* 1100–1101.
25. Feldman, Y.; Zak, A.; Popovitz-Biro, R.; Tenne, R. New reactor for production of tungsten disulfide hollow onion-like (inorganic fullerene-like) nanoparticles. *Solid State Sci.* **2000**, *2*, 663–672.
26. Feldman, Y.; Frey, G.L.; Homyonfer, M.; Lyakhovitskaya, V.; Margulis, L.; Cohen, H.; Hodes, G.; Hutchison, J.L.; Tenne, R. Bulk synthesis of inorganic fullerene-like MS_2 (M = Mo, W) from the respective trioxides and the reaction mechanism. *J. Am. Chem. Soc.* **1996**, *118*, 5362–5367.
27. Rothschild, A.; Sloan, J.; Tenne, R. Growth of WS_2 nanotubes phases. *J. Am. Chem. Soc.* **2000**, *122*, 5169–5179.
28. Dai, J.J.; Cui, H.P.; Grace, J.R. Biomass feeding for thermochemical reactors. *Prog. Energy Combust. Sci.* **2012**, *38*, 716–736.
29. Wilson, D.H.; Dunnington, D.L. Plan ahead to avoid feeding problems. *Chem. Eng. N. Y.* **1991**, *98*, 72–81.
30. Hao, X.H.; Guo, L.J.; Mao, X.; Zhang, X.M.; Chen, X.J. Hydrogen production from glucose used as a model compound of biomass gasified in supercritical water. *Int. J. Hydrogen Energy* **2003**, *28*, 55–64.
31. Deepak, F.L.; Tenne, R. Gas-phase synthesis of inorganic fullerene-like, structures and inorganic nanotubes. *Cent. Eur. J. Chem.* **2008**, *6*, 373–389.
32. Rosentsveig, R.; Margolin, A.; Feldman, Y.; Popovitz-Biro, R.; Tenne, R. WS_2 nanotube bundles and foils. *Chem. Mater.* **2002**, *14*, 471–474.
33. Margolin, A.; Rosentsveig, R.; Albu-Yaron, A.; Popovitz-Biro, R.; Tenne, R. Study of the growth mechanism of WS_2 nanotubes produced by a fluidized bed reactor. *J. Mater. Chem.* **2004**, *14*, 617–624.
34. Alaei, M.; Rashidi, A.; Mahjoub, A. Two suitable methods for the preparation of inorganic fullerene-like (IF) WS_2 nanoparticles. *Iran. J. Chem. Chem. Eng.* **2009**, *28*, 91–98.
35. Wiesel, I.; Arbel, H.; Albu-Yaron, A.; Popovitz-Biro, R.; Gordon, J.M.; Feuermann, D.; Tenne, R. Synthesis of WS_2 and MoS_2 fullerene-like nanoparticles from solid precursors. *Nano Res.* **2009**, *2*, 416–424.
36. Zhu, Y.Q.; Hsu, W.K.; Terrones, H.; Grobert, N.; Chang, B.H.; Terrones, M.; Wei, B.Q.; Kroto, H.W.; Walton, D.R.M.; Boothroyd, C.B.; *et al.* Morphology, structure and growth of WS_2 nanotubes. *J. Mater. Chem.* **2000**, *10*, 2570–2577.
37. Li, Y.H.; Zhao, Y.M.; Ma, R.Z.; Zhu, Y.Q.; Fisher, N.; Jin, Y.Z.; Zhang, X.P. Novel route to WO_x nanorods and WS_2 nanotubes from WS_2 inorganic fullerenes. *J. Phys. Chem. B* **2006**, *110*, 18191–18195.

38. Zhu, Y.Q.; Hu, W.B.; Hsu, W.K.; Terrones, M.; Grobert, N.; Hare, J.P.; Kroto, H.W.; Walton, D.R.M.; Terrones, H. Tungsten oxide tree-like structures. *Chem. Phys. Lett.* **1999**, *309*, 327–334.
39. Zak, A.; Sallacan-Ecker, L.; Margolin, A.; Feldman, Y.; Popovitz-Biro, R.; Albu-Yaron, A.; Genut, M.; Tenne, R. Scaling up of the WS_2 nanotubes synthesis. *Fullerenes Nanotubes Carbon Nanostruct.* **2011**, *19*, 18–26.
40. Zak, A.; Sallacan-Ecker, L.; Margolin, A.; Genut, M.; Tenne, R. Insight into the growth mechanism of WS_2 nanotubes in the scaled-up fluidized-bed reactor. *Nano* **2009**, *4*, 91–98.
41. Finnie, G.J.; Kruyt, N.P.; Ye, M.; Zeilstra, C.; Kuipers, J.A.M. Longitudinal and transverse mixing in rotary kilns: A discrete element method approach. *Chem. Eng. Sci.* **2005**, *60*, 4083–4091.